Oncogene (2021) 40:2258–2272
https://doi.org/10.1038/s41388-021-01701-z

ARTICLE

Statins repress hedgehog signaling in medulloblastoma with no bone toxicities

Qianhai Fan[1,2] · Tingting Gong[3] · Chaonan Zheng[1] · Jessica M. Y. Ng[4] · Jianquan Chen[3] · Cynthia Myers[5] · Harvey Hensley[6] · Tom Curran[4] · Zeng-jie Yang[2]

Received: 8 September 2020 / Revised: 30 January 2021 / Accepted: 5 February 2021 / Published online: 1 March 2021

Abstract

The Hedgehog (Hh) pathway plays an indispensable role in bone development and genetic activation of the pathway results in medulloblastoma (MB), the most common malignant brain tumor in children. Inhibitors of Hh pathway (such as vismodegib and sonedigib), which are used to treat MB, cause irreversible defects in bone growth in young children. Cholesterol is required for the activation of the Hh pathway, and statins, inhibitors of cholesterol biosynthesis, suppress MB growth by repressing Hh signaling in tumor cells. Here, we investigate the role of cholesterol biosynthesis in the proliferation and Hh signaling in chondrocytes, and examine the bone development in mice after statin treatment. Statins significantly inhibited MB growth in young mice, but caused no defects in bone development. Conditional deletion of NADP steroid dehydrogenase-like (NSDHL), an enzyme necessary for cholesterol biosynthesis, suppressed cholesterol synthesis in chondrocytes, and disrupted the growth plate in mouse femur and tibia, indicating the important function of intracellular cholesterol in bone development. Hh pathway activation and the proliferation of chondrocytes were inhibited by statin treatment in vitro; however, statins did not impair bone growth in vivo due to insufficient penetration into the bone. Our studies reveal a critical role of cholesterol in bone development, and support the utilization of statins for treatment of MB as well as other Hh pathway-associated malignancies.

Introduction

The Hedgehog (Hh) pathway is widely involved in patterning and morphogenesis of various organs during vertebrate development. In the conventional Hh signal transduction, the seven-pass transmembrane protein smoothened (Smo) is repressed by Patched1 (Ptch1), the antagonizing receptor of Hh ligand. *Ptch1* is frequently mutated in the Hh pathway-associated malignancies, including medulloblastoma (MB), the most common malignant brain tumor in children. *Ptch1* deficiency results in the release of Smo, which consequently activates Gli proteins, leading to elevated expression of Hh pathway target genes such as *Gli1/2* and *Ptch2* [1]. Conditional deletion of *Ptch1* in cerebellar granule neuron precursors, using *Math1-Cre/Ptch1*$^{fl/fl}$ mice, results in MB formation with 100% penetrance [2], providing an excellent model for preclinical studies of Hh pathway-associated MB.

Hh signaling plays an important role in endochondral ossification, a process in which cartilage molds are initially formed and replaced by bones [3, 4]. Endochondral ossification initiates with the condensation of mesenchymal stem

Supplementary information The online version contains supplementary material available at https://doi.org/10.1038/s41388-021-01701-z.

✉ Zeng-jie Yang
zengjie.yang@fccc.edu

1 Pediatric Cancer Center, College of Pharmaceutical Sciences, Soochow University, Suzhou, Jiangsu 215007, China

2 Cancer Biology Program, Fox Chase Cancer Center, Temple University Health System, Philadelphia, PA, USA

3 Orthopedic Institute, Medical College, Soochow University, Suzhou, Jiangsu 215007, China

4 Children's Research Institute, Children's Mercy Kansas City, Kansas City, MO, USA

5 Organic Synthesis Facility, Fox Chase Cancer Center, Temple University Health System, Philadelphia, PA, USA

6 Small Animal Imaging Facility, Fox Chase Cancer Center, Temple University Health System, Philadelphia, PA, USA

cells, which give rise to chondrocytes expressing Sox9 and type II collagen [5]. Then, chondrocytes undergo proliferation and differentiation within the growth plate. Chondrocyte maturation results in post-mitotic hypertrophy and the deposition of a calcified matrix [6]. Depending on the stage of differentiation, chondrocytes elaborate sequential layers in the growth plate: the resting zone, proliferation zone, and hypertrophic zone, respectively. Indian hedgehog (Ihh), secreted by prehypertrophic and hypertrophic chondrocytes, serves as the major Hh ligand to regulate endochondral ossification. Mice lacking *Ihh* or *Smo* in chondrocytes exhibit decreased number of chondrocytes [7, 8], indicating that Hh signaling promotes chondrocyte propagation in the growth plate.

Aberrant activation of Hh pathway is associated with malignancies such as MB and basal cell carcinoma (BCC) [9]. Approximately 30% of human MB cases have mutations in sonic hedgehog pathway (SHH-MB) [10, 11]. A majority of Hh pathway inhibitors, currently in preclinical and clinical studies, target Smo, including vismodegib (Genentech Inc.) and sonedigib (Novartis Inc.), which have been approved by the Federal Drug Administration (FDA). Despite initial dramatic responses to treatment with Smo inhibitors, tumors frequently develop resistance [12, 13]. Drug resistance arises primarily from activating mutations of Smo [14, 15] as well as mutations in the Hh pathway that lie downstream of Smo, including loss of SUFU and amplification of Gli1/2 [16, 17]. Moreover, due to the well-known functions of Hh signaling in bone development, Smo antagonists inhibit proliferation of chondrocytes and cause dramatic expansion of the hypertrophic zone, leading to premature fusion of the growth plate in mice [18]. Such defects in bone development in mice appear to be irreversible even after transient inhibition of Hh signaling. Following treatment with vismodegib or sonidegib, young patients with MB were found to develop widespread growth plate fusions that persist even after cessation of therapy [19, 20]. Currently, the FDA restricts the use of Smo inhibitors in young children prior to completion of bone growth.

Cholesterol is synthesized through a series of ~30 enzymatic reactions, starting with the substrate, acetyl-CoA. The enzyme 3-hydroxy-3-methylglutaryl-coenzyme A reductase (HMGCR) is rate limiting for cholesterol biosynthesis. HMGCR converts HMG-CoA to mevalonate and is the target for statins [21]. NADP steroid dehydrogenase-like (NSDHL), a 3β-hydroxysterol dehydrogenase, is involved in the synthesis of zymosterol from lanosterol. Dysfunction of NSDHL by either sporadic mutations or genetic deletion significantly impairs cholesterol biosynthesis [22, 23]. Cholesterol plays several important roles in the regulation of Hh signaling. Cholesterol is required for post-translational modification of Hh required for long-range signaling [24, 25]. Moreover, cholesterol itself was recently identified as an endogenous ligand for Smo [26, 27]. Structural studies further confirmed the interaction of cholesterol with the extracellular domain of Smo [28]. Recently we demonstrated that inhibition of cholesterol biosynthesis by using simvastatin or atorvastatin repressed Hh signaling and proliferation in MB cells [29]. Treatment with simvastatin or atorvastatin alone significantly reduced the growth of allograft mouse MB. These findings support the use of statins in the treatment of Hh pathway tumors. However, the effect of statin treatment on bone development remained an open question.

Here, we examined the effects of statins on Hh signaling in chondrocytes and on the growth of longitudinal bones in mice. No alterations in Hh pathway activation in chondrocytes were observed in mice after oral treatment with simvastatin. In addition, bone development in mice was not influenced by statin treatment, while MB growth in the brain was dramatically repressed. Our studies further revealed that the proliferation and Hh signaling in chondrocytes indeed relies on cholesterol biosynthesis. This is consistent with the finding that statins significantly suppress Hh signaling and inhibit the proliferation in chondrocytes in vitro. This apparent contradiction was resolved by mass spectrometry observations that there was insufficient penetration of statins into mouse cartilage. Thus, our studies provide an explanation for the lack of bone toxicity after statin treatment and they confirm the critical role of cholesterol in chondrocyte development, supporting the use of statins in the treatment of Hh pathway human malignancies, including MB and BCC.

Results

Simvastatin inhibits MB cell proliferation and tumor growth in young mice

To examine the tumor inhibitory effects of statins, we treated *Math1-Cre/Ptch1*$^{fl/fl}$ mice at P10 with 100 mg/kg simvastatin or vehicle (MCT) by oral gavage for seven consecutive days. The tumor size was examined by magnetic resonance imaging (MRI) following drug treatment. In addition, tumor-bearing mice were pulse-labeled with EdU for 1 h before fixation. As shown in Fig. 1a, b, the tumor volume was significantly reduced after treatment with simvastatin, compared with vehicle treatment. The decreased tumor size after simvastatin treatment was further confirmed by MRI analyses of brains from *Math1-Cre/Ptch1*$^{fl/fl}$ mice (Fig. 1c–e). These data suggest that simvastatin treatment significantly represses the in vivo growth of MB, consistent with our previous report [29]. As expected, tumor cells were readily detected on the surface of the *Ptch1*-deficient cerebellum following vehicle treatment, resulting in compromised cerebellar structures (Fig. 1f). However, the number of tumor cells in the mutant

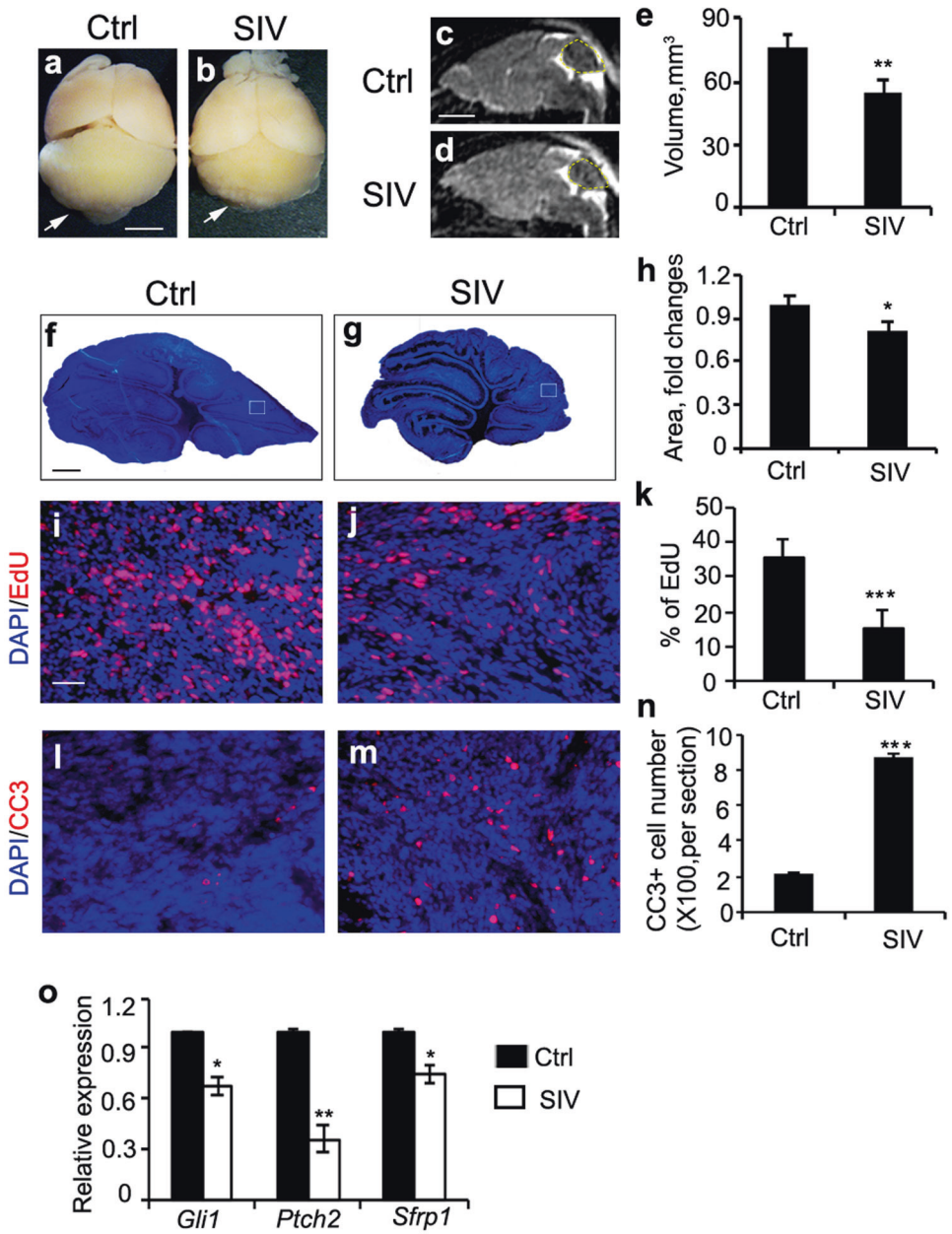

Fig. 1 Simvastatin inhibited the proliferation and Hh signaling in MB cells. *Math1-Cre/Ptch1*$^{fl/fl}$ mice at P10 were treated with 100 mg/kg simvastatin (SIV) or vehicle (MCT, Ctrl) by oral gavage once a day for seven consecutive days. **a**, **b** Whole-mount pictures of tumor-bearing brains after treatment with SIV or vehicle. Arrows point to tumors in mouse cerebella. **c**–**e** MRI images of brains from *Math1-Cre/Ptch1*$^{fl/fl}$ mice after treatment with SIV or vehicle. Yellow lines circle tumors in the cerebella. Tumor volume was quantified based on MRI images (**e**, $n = 5$). **f**–**h** DAPI staining of cerebellar sections prepared from *Math1-Cre/Ptch1*$^{fl/fl}$ mice after treatment with SIV or vehicle. Fold changes in tumor size after SIV treatment relative to that after vehicle treatment (Ctrl), based on the area of mid-sagittal cerebellar sections (**h**, $n = 6$). **i**–**n** Cerebellar sections from *Math1-Cre/Ptch1*$^{fl/fl}$ mice after treatment with SIV or vehicle were stained for EdU (**i**, **j**) or cleaved caspase-3 (CC3, **l**, **m**). **i** and **j** correlate with boxed regions in **f** and **g**, respectively. DAPI was used to counterstain cell nuclei. The percentage of EdU+ cells in cerebellar tissues and the number of CC3+ per cerebellar section were quantified in **k** and **n**, respectively ($n = 6$). **o** MB cells from *Math1-Cre/Ptch1*$^{fl/fl}$ mice after SIV or vehicle treatment were harvested to examine the mRNA expression of *Gli1*, *Ptch2*, and *Sfrp1* ($n = 5$). Values represent means ± s.d. in **e**, **h**, **k**, **n**, **o**. Scale bars: **a**, **b** 2 mm; **c**, **d** 4 mm; **f**, **g** 500 μm; **i**, **j**, **l**, **m** 25 μm.

cerebellum was markedly reduced after simvastatin treatment (Fig. 1g, h). More than 30% (30 ± 5%, $n = 5$) of MB cells were found positive for EdU in the cerebella after phosphate-buffered saline (PBS) treatment, whereas fewer than 15% (15 ± 4%, $n = 5$) of tumor cells were EdU+ in simvastatin-treated cerebella (Fig. 1i–k). These data indicate

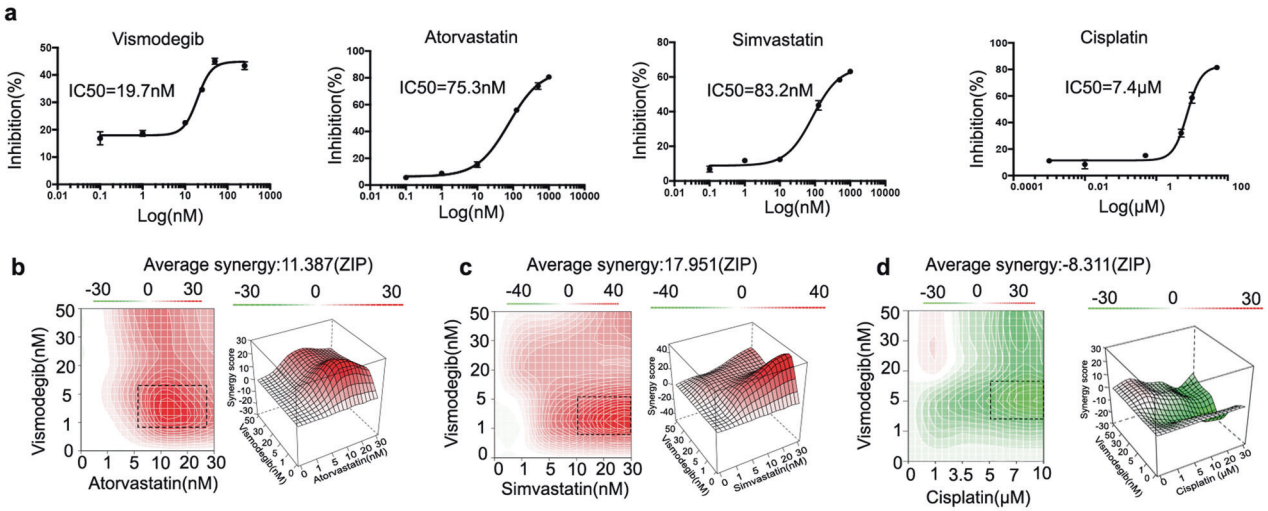

Fig. 2 Statins synergized with vismodegib in inhibiting MB cell proliferation. a IC_{50} values for vismodegib, atorvastatin, simvastatin, or cisplatin in inhibiting MB cell proliferation ($n = 6$). **b–d** The drug interaction landscapes based on the ZIP model. The interaction landscapes for the combinations of vismodegib and atorvastatin (**b**), simvastatin (**c**), or cisplatin (**d**) are shown in both 2D (left panel) and 3D (right panel). Synergy scores for each combination are color coded. A vertical box highlights the drug combinations with strongest synergistic effects (**b**, **c**) or antagonist effects (**d**).

that simvastatin treatment inhibited the proliferation of MB cells. The number of cells positive for cleaved caspase-3 was markedly increased in cerebellar tissues after treatment with simvastatin (Fig. 1l–n), suggesting that MB cell apoptosis was induced by simvastatin. In addition, cerebella from *Math1-Cre/Ptch1*$^{fl/fl}$ mice after treatment with simvastatin or PBS was harvested to examine the expression of Hh pathway target genes including *Gli1*, *Ptch2*, and *Sfrp1* by quantitative PCR (Q-PCR). As shown in Fig. 1o, the expression of *Gli1*, *Ptch2*, and *Sfrp1* mRNAs was significantly downregulated in the cerebella after simvastatin treatment, compared with vehicle treatment, suggesting that Hh signaling was compromised in mutant cerebella after simvastatin treatment. The above data demonstrate that simvastatin effectively suppresses tumor cell proliferation and Hh signaling in MB tissue. However, vismodegib repressed MB growth to a greater extent than simvastatin (both drugs at 50 mg/kg, Supplementary Fig. 1), suggesting that vismodegib is more potent in inhibiting tumor growth compared with simvastatin.

Recent studies reveal the direct interaction of cholesterol with the transmembrane domain of Smo containing the binding site of vismodegib [28, 30, 31]. These findings suggest that statins may synergize vismodegib in inhibiting MB cell proliferation. To test this, we isolated MB cells from *Math1-Cre/Ptch1*$^{fl/fl}$ mice at 6 weeks of age, and treated them in vitro with vismodegib, atorvastatin, or simvastatin at different concentrations. MB cells were treated with vehicle (DMSO) as a control. Cisplatin, a potent chemotherapeutic agent used in standard MB protocol, was also used to treat MB cells as a control. The survival of MB cells was measured by Cell Counting Kit-8 (CCK8) at 48 h following the treatment. The IC_{50} values for each drug in MB cells were calculated as following: vismodegib, $IC_{50} = 19.7$ nM; atorvastatin, $IC_{50} = 75.3$ nM; simvastatin, $IC_{50} = 83.2$ nM; cisplatin, $IC_{50} = 7.4$ μM (Fig. 2a). We then treated MB cells with vismodegib combined with atorvastatin, simvastatin, or cisplatin for 48 h. The cell viability data were used to determine the drug interaction by SynergyFinder, a web application for analyzing the drug combination dose–response data [32–34]. The zero interaction potency (ZIP), a reference model, was used to score the drug interaction relationships by comparing the change in the potency of the dose–response curves between individual drugs and their combination [35]. ZIP score >10 suggest synergism and scores <−10 indicate antagonism. ZIP scores between −10 and 10 suggest the interaction of two drugs is additive. As shown in Fig. 2b, c, the synergistic effects were found in the combination of vismodegib and atorvastatin or simvastatin. The strongest synergism effect was found within the region of dose combination where the dose of vismodegib was relatively low (1–5 nM). However, the interaction of vismodegib and cisplatin was overall additive (score: −8.311). Cisplatin at high doses (5–10 μM) appeared to be antagonistic with vismodegib (Fig. 2d). These data further confirm that statins can synergize with vismodegib in repressing MB cell proliferation, in agreement with our previous report [29].

No bone toxicities are caused by simvastatin treatment

To examine the possible toxicities of statins in bone development, we then treated *Math1-Cre/Ptch1*$^{fl/fl}$ mice at P10 with 100 mg/kg simvastatin or vehicle (MCT) once a

day for seven consecutive days. In addition, *Math1-Cre/Ptch1*$^{fl/fl}$ mice were treated with 50 mg/kg vismodegib as a positive control. Following the drug treatment, tumor-bearing mice were scanned by Positron emission tomography-computed tomogography (PET-CT) to measure the length of femur and tibia bones. As shown in Fig. 3a–c, similar lengths of mouse femur and tibia were found in control mice and mice treated with simvastatin, suggesting that no obvious defects were induced by simvastatin treatment. As expected, femur bones were significantly shortened in mice after vismodegib treatment, compared with vehicle treatment (Fig. 3d). Chondrocytes are organized into different zones in the growth plate including resting zone, proliferation zone, and hypertrophic zone (Fig. 3e). We then analyzed mouse tibia using an antibody against collagen type II (Col2), a marker for chondrocytes [36]. The cellular organization and the thickness of the growth plate of mouse femur bones were not altered after treatment with simvastatin, compared with vehicle treatment. However, the chondrocyte population dropped significantly and the growth plate became much thinner after vismodegib treatment, consistent with the critical role of the Hh pathway in development of the growth plate (Fig. 3f–i). In addition, the percentage of EdU+ cells in the proliferative zone of either femur or tibia was comparable after simvastatin treatment or vehicle treatment, although vismodegib significantly reduced the number of EdU+ cells in the femur and tibia (Fig. 3j–p). These data suggest that proliferation of chondrocytes and growth plate development are not affected by simvastatin treatment. Moreover, comparable levels of *Gli1*, *Ptch2*, and *Sfrp1* mRNA expression were detected in cartilage from mouse femur following treatment with simvastatin or vehicle, although vismodegib significantly repressed the expression of Hh pathway genes in chondrocytes (Fig. 3q). Consistent with our previous report [18], vismodegib treatment inhibited proliferation and promoted differentiation of chondrocytes leading to a reduced proliferative zone and expanded hypertrophic zone (ColX+) in the growth plate of mouse tibia (Supplementary Fig. 2a–i). However, the structure of the growth plate in mice after simvastatin treatment is indistinguishable from that in control mice. These findings indicate that Hh signaling in chondrocytes is not affected by simvastatin treatment in vivo.

To examine whether simvastatin caused any possible long-term defects in bone development, we treated the *Math1-Cre/Ptch1*$^{fl/fl}$ mice at P10 with 100 mg/kg simvastatin, 50 mg/kg vismodegib or vehicle as controls for 7 days. After the treatment, the growth of mouse femur and tibia were examined by PET-CT once a week until 8 weeks of age. As shown in Fig. 3r, s, at 8 weeks of age, no difference in the length of the femur and tibia was observed in mice after simvastatin treatment, compared with PBS treatment, suggesting that no long-term defects in bone development were caused by simvastatin treatment. As a comparison, the femur was still markedly shortened in mice following the treatment with vismodegib (Fig. 3t–u). Similarly, tibia growth was significantly suppressed by vismodegib, whereas tibia lengths observed after treatment with simvastatin were comparable to those of control mice (Fig. 3v). In addition, severely disrupted growth plates were observed in the cartilages examined at 8 weeks following vismodegib treatment. In contrast, no defects were found in the growth plate after treatment with vehicle or simvastatin (Supplementary Fig. 2j–l). These data indicate that simvastatin causes no long-term defects in mouse cartilage.

Simvastatin represses Hh signaling in chondrocyte in vitro

Having observed that simvastatin caused no defects in chondrocyte proliferation as well as bone development in vivo, we next examined whether the proliferation of chondrocytes can be repressed by statin treatment in vitro. For this purpose, we isolated chondrocytes from mice at p5, and treated with PBS, Shh conditioned medium (Shh-CM), or Shh-CM combined with vismodegib. At 48 h following treatment, chondrocytes were harvested to examine proliferation and Hh signaling by immunocytochemistry and Q-PCR, respectively. As shown in Fig. 4a, spontaneous proliferation (Ki67+) was detected in chondrocytes in the control culture (with PBS). The addition of Shh-CM markedly increased proliferation (Ki67+) of chondrocytes, whereas Shh-induced proliferation of chondrocytes was significantly inhibited by vismodegib (Fig. 4b). In addition, expression of *Gli1* mRNA was elevated in chondrocytes following the treatment with Shh-CM, indicating that the Hh pathway was activated in chondrocytes upon the Shh-CM treatment. Expression levels of *Gli1* mRNA were significantly declined in chondrocytes after treatment with Shh-CM together with vismodegib, compared with the treatment with Shh-CM alone (Fig. 4c). The above data indicate that activation of the Hh pathway promotes proliferation of chondrocytes.

To examine whether statins can inhibit chondrocyte proliferation in vitro, we next treated chondrocytes with Shh-CM in the presence of 10 μM simvastatin, 10 μM atorvastatin or PBS as a control. After the treatment for 48 h, chondrocytes were collected to examine proliferation by immunocytochemistry (Fig. 4d). As shown in Fig. 4e, the percentage of Ki67+ cells markedly decreased in cultures following treatment with simvastatin or atorvastatin. Similarly, expression levels of *Gli1* were significantly suppressed in chondrocytes after treatment with simvastatin or atorvastatin, compared with PBS treatment (Fig. 4f). These data suggest that statins treatment inhibited Hh signaling transduction in chondrocytes, and repressed chondrocytes proliferation. In addition, levels of intracellular cholesterol were

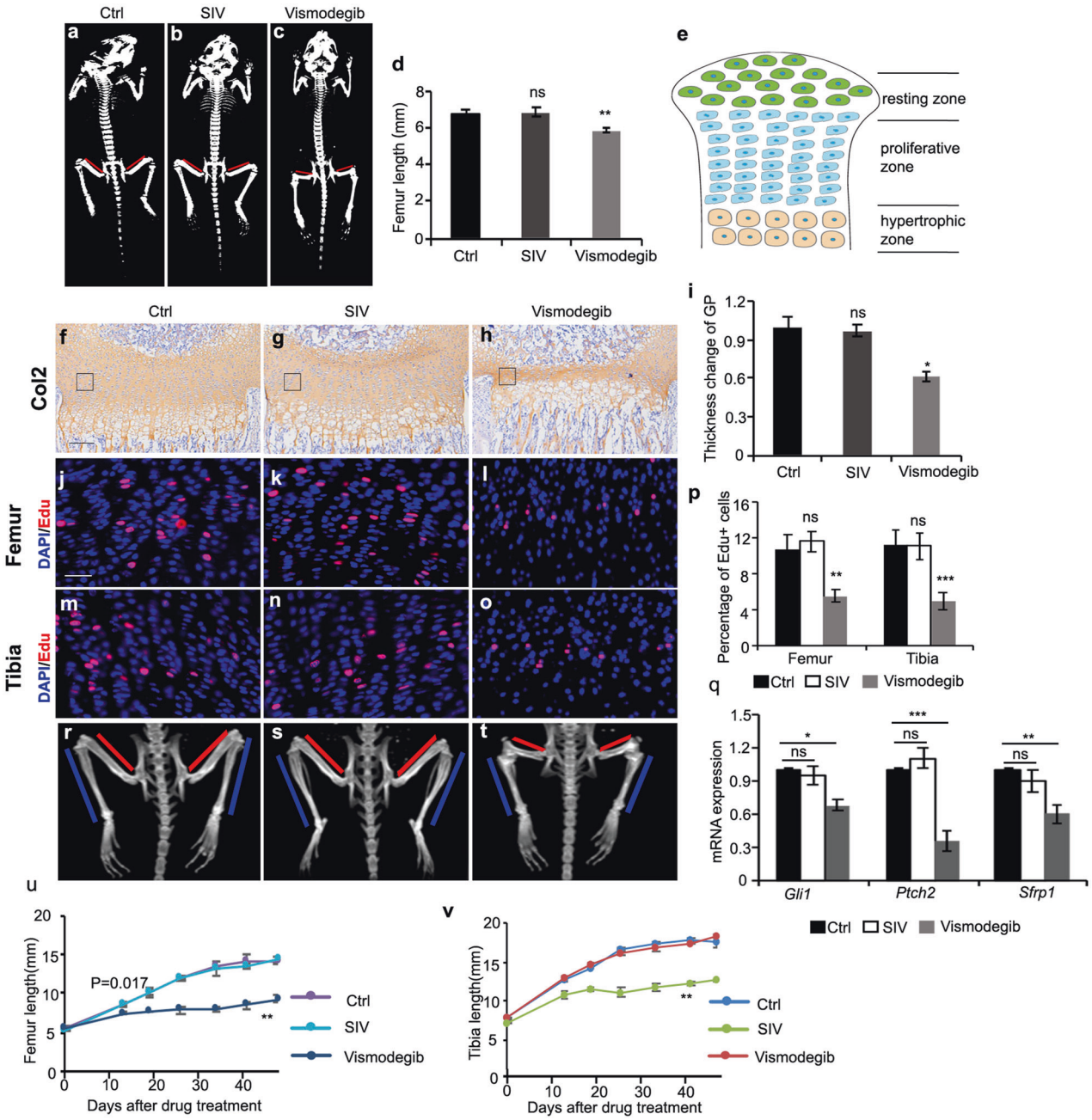

Fig. 3 No bone defects were detected in mice after simvastatin treatment. *Math1-Cre/Ptch1*$^{fl/fl}$ mice at P10 were treated with PBS, 100 mg/kg simvastatin (SIV), or 50 mg/kg vismodegib for seven consecutive days. **a**–**d** Tumor-bearing mice were scanned by PET-CT at P17 after drug treatment. Red lines show the length of femur, which are quantified in **d** ($n = 5$). **e** Schematic diagram of a longitudinal section through the epiphyseal growth plate. **f**–**q** Femurs (**f**–**h**, **j**–**l**) and tibias (**m**–**o**) were collected from tumor-bearing mice after drug treatment to examine the growth plate (Col2+, **f**–**h**) and proliferation of chondrocytes (EdU+, **j**–**l**, **m**–**o**) by immunohistochemistry. The thickness of growth plate (GP) and percentage of EdU+ chondrocytes was quantified in **i** and **p**, respectively ($n = 6$). Cartilages after drug treatment were collected to examined the expression of Hh pathway genes (*Gli1*, *Ptch2*, and *Sfrp1*) by Q-PCR. The levels of Hh pathway gene expression after drug treatment, relative to those in vehicle control, were shown in **q** ($n = 6$). **r**–**v** *Math1-Cre/Ptch1*$^{fl/fl}$ mice at P10 were treated with vehicle, 100 mg/kg SIV or 50 mg/kg vismodegib for seven consecutive days, and scanned by PET-CT once a week until 8 weeks of age. PET-CT images of femur and tibia from tumor-bearing mice at 8 weeks of age (**r**–**t**). Red lines and blue lines show the length of femur and tibia, respectively. Dynamic changes in the length of femur and tibia after drug treatment were shown in **u** and **v** ($n = 6$). Values are means ± s.d. in **d**, **I**, **p**, **q**, **u** and **v**. Scale bars: **f**–**h**, 100 μm; **j**–**o**, 25 μm.

reduced in chondrocytes following treatment with simvastatin or atorvastatin, as expected (Fig. 4g). To further test whether statins-repressed proliferation of chondrocytes can be rescued by cholesterol, we treated chondrocytes with vehicle, Shh-CM combined with simvastatin or atorvastatin in the absence/presence of 13 μM water-soluble cholesterol

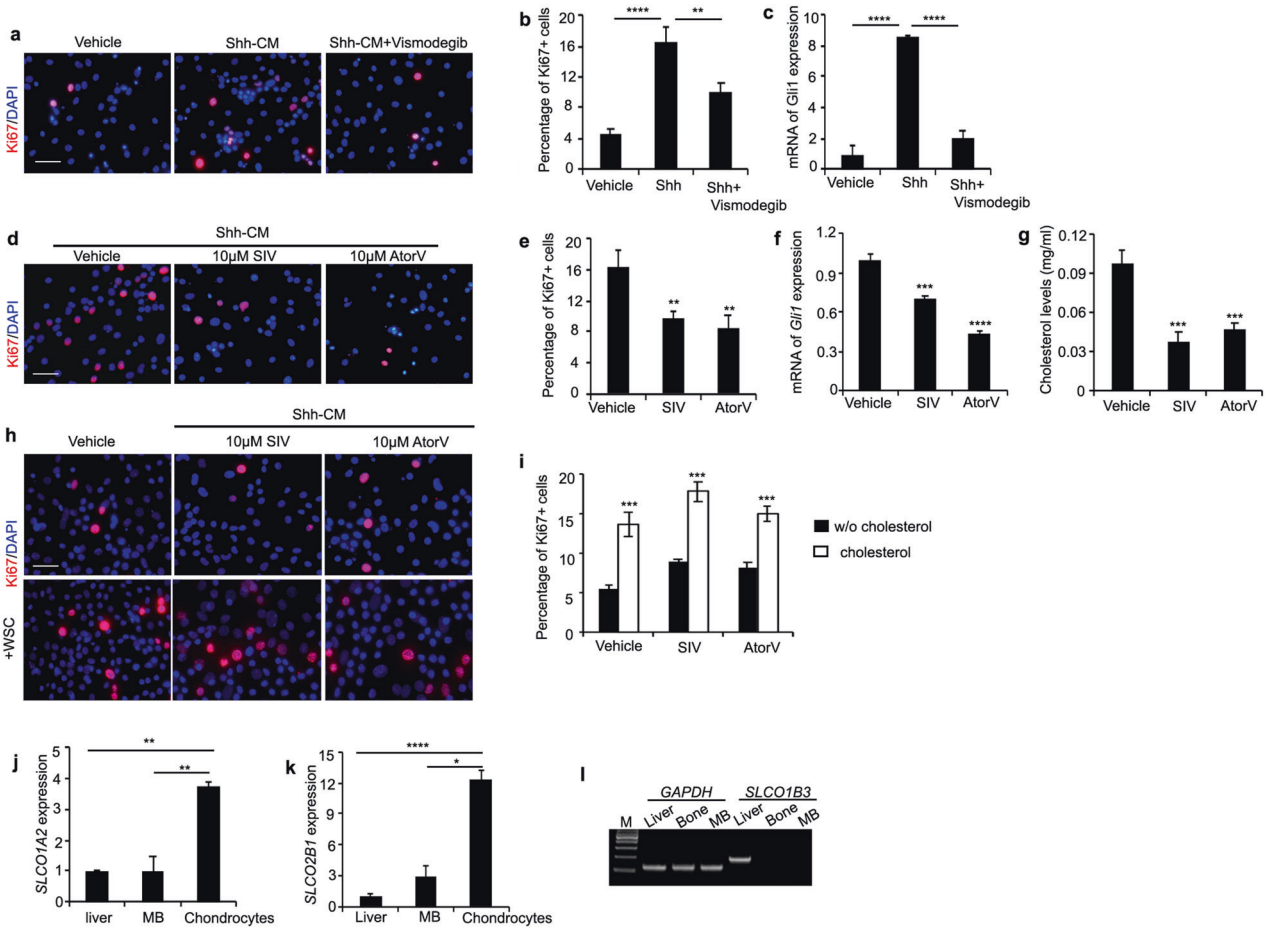

Fig. 4 Statins inhibited chondrocyte proliferation in vitro. a–c Chondrocytes isolated from wild-type mice at P5 were treated with PBS, 15% Shh-CM, or 15% Shh-CM together with 200 nM vismodegib for 48 h, and harvested to examine their proliferation (Ki67+, **a**) by immunocytochemistry and *Gli1* mRNA expression by Q-PCR. DAPI was used to counterstain cell nuclei. The percentage of Ki67+ cells and expression levels of *Gli1* were quantified in **b** and **c**, respectively ($n = 6$). **d–g** Chondrocytes from wild-type mice at P5 were treated with 15% Shh-CM combined with vehicle, 10 μM simvastatin, or 10 μM atorvastatin for 48 h. Following the treatment, chondrocytes were harvested to examine the proliferation by immunocytochemistry (**d**), measure cholesterol levels and *Gli1* expression by Q-PCR. The percentage of Ki67+ cells, the levels of *Gli1* mRNA expression, and cholesterol levels (normalized by the total amount of proteins) were quantified in **e**, **f**, and **g**, respectively ($n = 5$). **h–i** Chondrocytes from wild-type mice at P5 were treated with vehicle, 15% Shh-CM combined with 10 μM simvastatin or 10 μM atorvastatin in the absence/presence of 13 μM water-soluble cholesterol (WSC) for 48 h, before being harvested for immunocytochemistry (**h**). The percentage of Ki67+ cells was shown in **i** ($n = 6$). **j–l** Relative expression levels of *SLCO1A2* and *SLCO2B1* in chondrocytes and MB tissues, normalized by that in liver tissue, examined by Q-PCR (**j**, **k**) ($n = 5$). Gel electrophoresis image of PCR products of *SLCO1B3* in MB tissue, liver tissue, and chondrocytes (**l**). GAPDH product was used for an internal control (**l**). Values represent means ± s.d. in **b**, **c**, **e–g**, **i**, **j**, **k**. Scale bars: 30 μm.

(WSC) for 48 h. As shown in Fig. 4h, cholesterol alone increased the proliferation of chondrocytes compared with the vehicle control. The addition of cholesterol significantly enhanced the percentage of Ki67+ cells in chondrocytes treated with statins (Fig. 4i). These data suggest that statin repression of chondrocyte proliferation is a consequence of cholesterol deficiency.

The cellular uptake of statins is mediated by organic anion transporting polypeptides (OATPs), especially OATP1A2, OATP2B1, and OATP1B3 that are encoded by solute carrier organic anion transporter family genes, member 1A2 (*SLCO1A2*), 2B1 (*SLCO2B1*), and 1B3 (*SLCO1B3*), respectively [37, 38]. Extensive expression of SLCO family genes is common in numerous tissues, particularly the liver [39]. We then examined the expression of *SLCO1A2*, *SLCO2B1*, and *SLCO1B3* in chondrocytes by Q-PCR. Mouse MB and liver tissues were used as controls. As shown in Fig. 4j, k, expression of both *SLCO1A2* and *SLCO2B1* mRNAs were significantly upregulated in chondrocytes, compared with that in liver or MB tissues. Interestingly, *SLCO1B3* expression appeared to be specific to liver tissue, with no expression detected in either MB tissue or chondrocytes (Fig. 4l). These data indicate that chondrocytes express OATPs required for the uptake of statins.

Cholesterol biosynthesis is critical for bone development

We next examined whether cholesterol is required for the proliferation and Hh signaling in chondrocytes. For this purpose, we investigated the possible alterations in bone development after genetic inhibition of cholesterol biosynthesis in chondrocytes. To target chondrocytes, we utilized *Sox9-CreER*^{T2} (*SCE*) mice in which Sox9+ cells carry an inducible Cre recombinase [40]. After crossing *SCE* mice with *Rosa-tdTomato* mice that have a loxp-flanked STOP cassette preventing transcription of red fluorescent protein variant (*tdTomato*) [41], the majority of chondrocytes (Sox9 +) were found to be positive for Tomato in the tibia from *SCE/Rosa-tdTomato* mice (Fig. 5a), suggesting that *SCE* mice can be utilized to target chondrocytes. We then crossed *SCE* mice with *NSDHL*$^{fl/fl}$ mice that harbor a conditional *NSDHL* allele [42], and treated *SCE/NSDHL*$^{fl/fl}$ mice at P10 with tamoxifen intraperitoneally (once a day for four consecutive days). *SCE* mice, *SCE/NSDHL*$^{fl/wt}$ mice, and wild-type mice at P10 were also treated with tamoxifen as controls. We isolated cartilages from the above mice after the tamoxifen treatment, and examined the *NSDHL* gene by PCR (Fig. 5b). As shown in Fig. 5c, the PCR band characteristic of deleted *NSDHL* was readily detected in cartilage from *SCE/NSDHL*$^{fl/fl}$ mice or *SCE/NSDHL*$^{fl/wt}$ mice, whereas it was not found in cartilage from wild-type mice or *SCE* mice. These data suggest that the *NSDHL* gene was effectively deleted in cartilage from *SCE/NSDHL*$^{fl/fl}$ mice following tamoxifen treatment. We next measured the cholesterol levels in cartilage from *SCE/NSDHL*$^{fl/fl}$ mice and *SCE* mice after tamoxifen treatment, using a cholesterol measurement assay as previously described [29]. The cholesterol levels were significantly reduced in chondrocytes from *SCE/NSDHL*$^{fl/fl}$ mice, compared with *SCE* mice (Fig. 5d), suggesting that *NSDHL* deletion effectively repressed intracellular cholesterol biosynthesis in chondrocytes.

We scanned *SCE/NSDHL*$^{fl/fl}$ mice and *SCE* mice at P16 after tamoxifen treatment by PET-CT. As shown in Fig. 5e, endochondral bones were overall shortened in *SCE/NSDHL*$^{fl/fl}$ mice compared with those in *SCE* mice. In particular, the length of tibia and femur was significantly decreased in *SCE/NSDHL*$^{fl/fl}$ mice compared with that in *SCE* mice (Fig. 5f). We then harvested tibia from *SCE/NSDHL*$^{fl/fl}$ mice and *SCE* mice for histological analyses. As shown in Fig. 5g, *NSDHL*-deficient tibia in *SCE/NSDHL*$^{fl/fl}$ mice were smaller in all dimensions compared with tibia from *SCE* littermates. The secondary ossification center (SOC) was already established in the control tibia at P16, whereas the SOC formation in tibia from *SCE/NSDHL*$^{fl/fl}$ mice was delayed. The growth plate organization was still visible in *NSDHL*-deficient tibia, except that the hypertrophic zone became much smaller after *NSDHL* deletion (Fig. 5g). The reduced hypertrophic zone in *NSDHL*-deficient tibia was more evident after safranin O staining (Fig. 5h), consistent with the disordered hypertrophic zone observed in fetal limb lacking SREBP cleavage-activating protein (SCAP), which acts as a cholesterol sensor regulating intracellular cholesterol biosynthesis [43]. Moreover, the number of EdU+ cells in chondrocytes located in the proliferation zone of either femur or tibia were significantly reduced after *NSDHL* loss, compared with those in the control mice (Fig. 5i, j). The markedly decreased percentage of EdU+ cells among chondrocytes following *NSDHL* deletion indicates that proliferation of chondrocytes was reduced after cholesterol biosynthesis was repressed (Fig. 5k). Finally, we isolated cartilages from *SCE/NSDHL*$^{fl/fl}$ mice and SCE mice after the tamoxifen treatment to examine the expression of Hh pathway target genes such as *Gli1* and *Sfrp1* by Q-PCR. As shown in Fig. 5l, expression levels of *Gli1* and *Sfrp1* mRNAs were significantly declined in chondrocytes after *NSDHL* deletion, suggesting that Hh signaling in cartilage was suppressed after inhibition of cholesterol biosynthesis. The above data confirm that intracellular cholesterol biosynthesis is required for the proliferation and Hh signaling in chondrocytes.

Simvastatin is not capable of penetrating into bone tissue

The above studies demonstrate a critical role for cholesterol in chondrocyte development. However, defects in chondrocyte development were not observed in mice after statin treatment. These observations led us to postulate that statins may be incapable of penetrating into the bone. To test this hypothesis, we examined whether simvastatin treatment could affect cholesterol levels in bone by treating *Math1-Cre/Ptch1*$^{fl/fl}$ mice at P10 with simvastatin or vehicle for 7 days. After treatment, we collected the plasma, MB tissue as well as cartilages to examine cholesterol levels using the cholesterol measurement kit. As shown in Fig. 6a–c, the levels of cholesterol in the plasma significantly declined after simvastatin treatment, as expected. A marked reduction in the cholesterol levels was also observed in the tumor tissue following the simvastatin treatment, in agreement with observations that simvastatin inhibits in vivo proliferation of MB cells. However, cholesterol levels were not altered in the bone after treatment with simvastatin or vehicle, indicating that cholesterol biosynthesis was not affected in bone by simvastatin treatment, possibly due to insufficient penetration of simvastatin in the bone.

To directly evaluate the penetration of simvastatin in different tissues, we examined simvastatin in the plasma, cerebella, and bone from wild-type mice by high-performance liquid chromatography (HPLC) and mass spectrometry (MS). Simvastatin is a prodrug that is hydrolyzed in vivo to generate

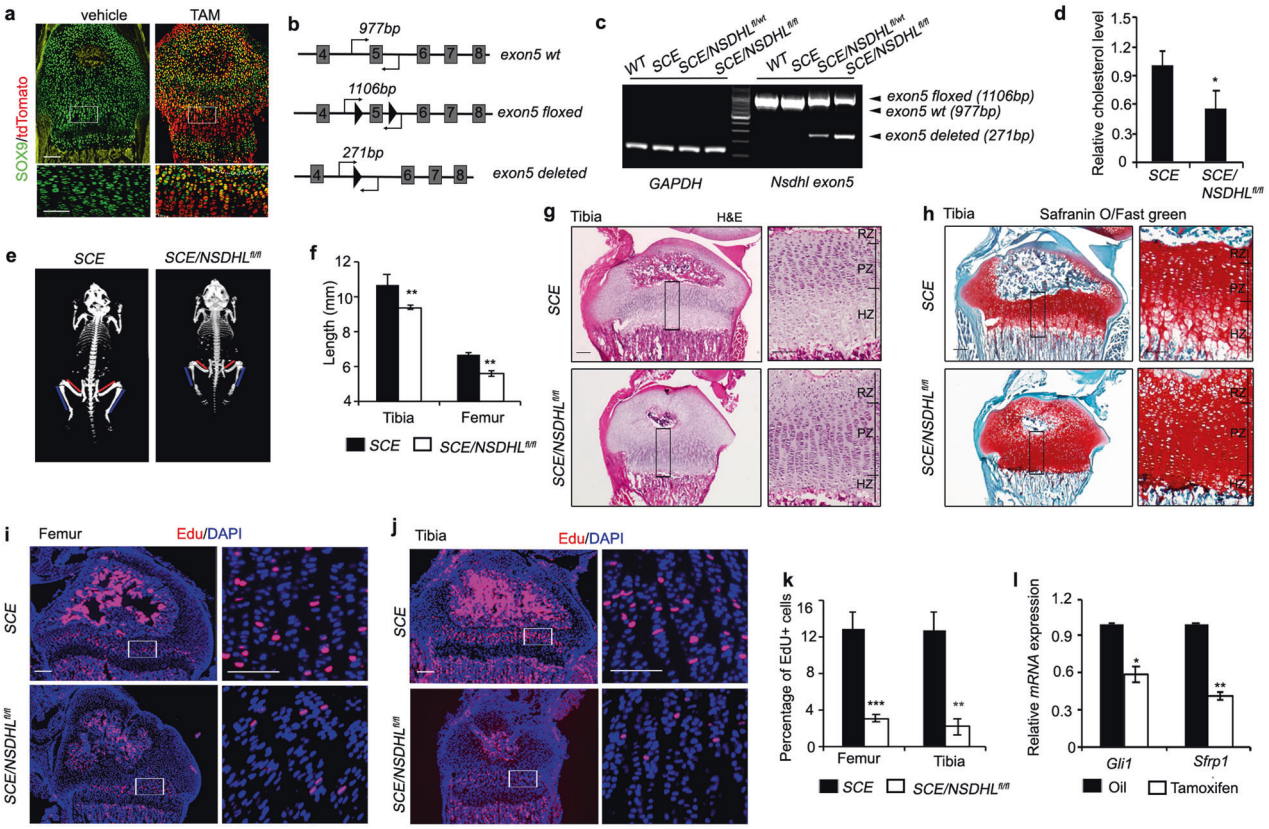

Fig. 5 Deficiency in cholesterol biosynthesis inhibited chondrocyte proliferation. **a** *Sox9-CreER^{T2}/Rosa-tdTomato* mice at P10 were treated with corn oil (vehicle) or tamoxifen by I.P. once a day for 4 days. Sections from mouse femur were prepared to examine Sox9 (green) and tomato (red) by immunohistochemistry. Lower panels show the magnified regions of the growth plate (boxed regions in upper panels). **b** Schematic diagram of wild type (wt), floxed as well as deleted *NSDHL* gene. Loxp sites flanking exon 5 of *NSDHL* gene are shown. Locations of PCR primers as well as the expected size of PCR products are labeled. **c** Cartilages isolated from femur of wild-type mice (*wt*), *Sox9-CreER^{T2}* mice (*SCE*), *Sox9-CreER^{T2}/NSDHL$^{fl/wt}$* (*SCE/NSDHL$^{fl/wt}$*) mice, and *Sox9-CreER^{T2}/NSDHL$^{fl/fl}$* (*SCE/NSDHL$^{fl/fl}$*) mice at P16 after tamoxifen treatment for 4 days were used to examine the presence of exon 5 of *NSDHL* gene. **d** The levels of cholesterol in cartilages harvested from SCE/*NSDHL$^{fl/fl}$* mice, relative to that from SCE mice after tamoxifen treatment ($n = 5$). **e, f** *SCE/NSDHL$^{fl/fl}$* mice and *SCE* mice at P16 after tamoxifen treatment for 4 days were scanned by PET-CT. Red lines and blue lines represent the length of femurs and tibias, respectively, which is quantified in **f** ($n = 6$). **g, h** Tibia of *SCE/NSDHL$^{fl/fl}$* at P16 following treatment with corn oil or tamoxifen for 4 days was collected for H&E staining (**g**) and safranin O staining (**h**). Fast green was used to counterstain the non-collagen region in the bone (**h**). Right panels show the magnified regions of the growth plate (boxed regions in left panels). **i–l** Femurs and tibias from *SCE/NSDHL$^{fl/fl}$* at P16 following treatment with corn oil or tamoxifen for 4 days were sectioned to examine the EdU incorporation by staining (**i**, **j**). DAPI was used to counterstain cell nuclei. Right panels show the magnified regions of the growth plate (boxed regions in left panels). The percentage of EdU+ cells in a growth plate was quantified in **k** ($n = 7$). Relative expression of *Gli1* and *Sfrp1* in cartilages from *SCE/NSDHL$^{fl/fl}$* mice at P14 after the treatment with tamoxifen or corn oil (**l**, $n = 5$). Values represent means ± s.d. in **d**, **f**, **k**, and **l**. Scale bars: **a** 100 μm; **g**, **h** 200 μm; **i**, **j** 200 μm.

simvastatin acid, an active metabolite potently competing with HMG-CoA [44]. As a control, vismodegib was also analyzed in the tissues by HPLC-MS. As shown in Fig. 6d, vismodegib, simvastatin, and simvastatin acid can be identified by their characteristic ultraviolet (UV) absorption spectra. We then harvested the plasma, cerebella, and bone from wild-type mice at 1 h following treatment with vismodegib or simvastatin. Vismodegib was readily detected in the plasma, cerebella, and bone, and the peak identification of vismodegib was confirmed in biological samples by high-resolution MS (Fig. 6e). These data indicate that vismodegib can effectively penetrate cerebellar tissues and bone, explaining the effective inhibition of Hh pathway in mouse cerebella and bone after oral treatment with vismodegib. Consistent with previous reports [45, 46], within 2 h after treatment with simvastatin (100 mg/kg), we were not able to detect simvastatin in mouse plasma, cerebella, or bone by HPLC-MS (data not shown), which may be due to the relative short half-life of simvastatin (~2 h) [47]. Peak levels of simvastatin acid were found in the plasma and cerebellum from wild-type mice after oral treatment of simvastatin acid by HPLC-MS (Fig. 6f). However, no simvastatin acid was detected in bone (Fig. 6f), indicating that there was insufficient penetration of simvastatin acid into bone tissues.

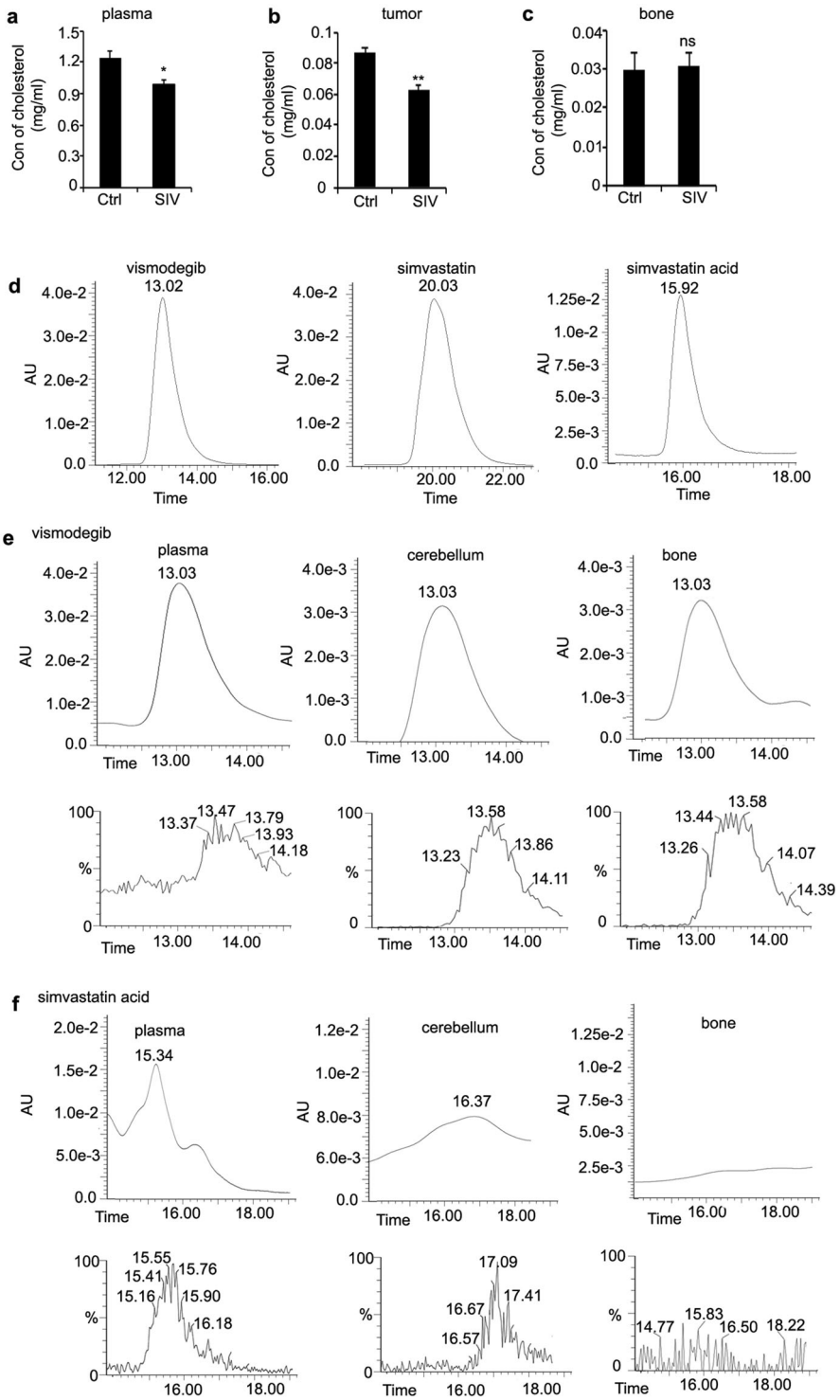

Fig. 6 Penetration of simvastatin in brain and bone. **a**–**c** *Math1-Cre/Ptch1*$^{fl/fl}$ mice at P10 were treated with vehicle or 100 mg/kg simvastatin for 7 days. Plasma, tumor tissues, and bones were collected from *Math1-Cre/Ptch1*$^{fl/fl}$ mice at P16 to examine cholesterol levels by the enzymatic assay. The amount of total protein from tissues was used to normalize the cholesterol concentrations ($n = 5$). Values are means ± s.d. **d** HPLC chromatograms of standard vismodegib, simvastatin, or simvastatin acid. **e** HPLC chromatograms of vismodegib present in the plasma, cerebellum, or bone of wild-type mice after oral gavage of vismodegib (50 mg/kg, for one time treatment). Lower panels show the chromatography of vismodegib in designated samples analyzed by MS. **f** HPLC chromatograms of simvastatin acid in the plasma, cerebellum, or bone of wild-type mice after oral gavage of simvastatin. Lower panels show the chromatography of simvastatin acid in designated samples analyzed by MS.

Discussion

Permanent defects in bone development caused by Smo inhibitors are considered on-target toxicity (also referred to as mechanism-based toxicity), in that chondrocyte proliferation and differentiation rely on Hh signaling [18]. Such toxicity in bone growth prevents the use of Smo inhibitors in young patients with MB or BCC. Here, we demonstrated that simvastatin causes no defects in bone development, despite the fact that it represses Hh signaling transduction in MB tissue in mouse brain. Our studies revealed that insufficient penetration into bone tissue prevented statins from inhibiting Hh signaling and proliferation of chondrocytes. Indeed, several cohort studies support the safety of statin use

in childhood [48]. In particular, in the study by Kusters et al. [49], no adverse events including bone defects were found in statin-treated children after a 10-year follow-up.

Dysregulation of cholesterol biosynthesis and homeostasis is involved in many human skeletal abnormalities [50]. In the current studies, conditional deletion of *NSDHL* in chondrocytes significantly reduced cholesterol levels in long bones. Moreover, deficiency in cholesterol biosynthesis inhibited proliferation of chondrocytes in the growth plate and disrupted ossification in femoral and tibial epiphysis. Hh signaling in the chondrocytes was markedly impaired after *NSDHL* deletion. These findings demonstrate the important role of intracellular biosynthesis of cholesterol in proliferation and Hh signal transduction in chondrocytes. In addition, these results suggest that cholesterol in bone primarily relies on intracellular synthesis in chondrocytes. Consistent with previous studies, embryonic deletion of *SCAP*, a sensor of intracellular cholesterol, resulted in reduced cholesterol biosynthesis in chondrocytes as well as disordered growth plates [43]. A recent study revealed that disruption of either *Dhcr7* (encoding an enzyme involved in cholesterol synthesis) or *Insig1* and *Insig2* (encoding proteins inhibiting cholesterol synthesis) compromised osteoblast differentiation and proliferation through primary cilium formation [51]. In our studies, the hypertrophic zone was reduced in the growth plates in *SCE/NSDHL*$^{fl/fl}$ mice after tamoxifen treatment. However, the expansion of the hypertrophic zone was observed in the growth plate after genetic or pharmaceutical inhibition of Hh pathway [7, 8, 18]. Potentially, deficiency in cholesterol synthesis inhibited chondrocytes differentiation/maturation independent of the Hh pathway, besides affecting the proliferation of chondrocytes by interfering Hh signaling.

Although MB can exhibit initial responses to Smo antagonists, including vismodegib and sonidegib, there is rapid emergence of drug resistance [12, 13]. Whether resistance occurs in MB cells after statin treatment remains to be addressed. Vismodegib impaired the development of mouse long bones including the tibia and femur [18]. However, no defects in cranial bones were detected in mice after vismodegib treatment. This could be due to the different role of Hh signaling in endochondral ossification (responsible for long bone development in the limb) and intramembranous ossification (mainly to support cranial bone development). It is well established that the Hh signaling pathway is essential for endochondral ossification. Disrupted endochondral ossification was observed in *Ihh −/−* mice as well as chondrocyte-specific *Smo−/−* mice [7, 52]. However, Hh signaling appears to be dispensable for intramembrane ossification. *Ihh−/−* mice developed small but relatively normal calvaria, and intramembrane ossification was not affected in cranial bones. Similarly, small but normal skulls were found in mice deficient for *Smo*. A recent study revealed that Gα signaling regulated Hh signaling in a ligand-independent manner during normal intramembrane bone formation [53]. Gαs, a heterotrimeric G protein, was found to repress intramembrane ossification by inhibiting Hh signaling downstream of Smo [53]. These findings provide a new conceptual framework to understand the functions of Hh signaling during craniofacial bone formation, which also explains the lack of defects in craniofacial bones after treatment with Smo inhibitors.

In our studies, simvastatin treatment significantly lowered the cholesterol levels in mouse plasma and cerebella, but not in the bone. The HPLC-MS analyses further revealed the insufficient penetration of simvastatin acid in bones from mice treated with simvastatin. As a comparison, vismodegib was readily detected in the plasma, brain as well as bone. However, inhibitors of cholesterol synthesis such as AY 9944 and triparanol induced limb anomalies in humans and rodents [54, 55], suggesting that these inhibitors may be capable of infiltration into the bone. Nevertheless, both AY 9944 and triparanol are not clinically applicable due to their severe side effects [56, 57]. Our studies by HPLC-MS analyses revealed a failure of simvastatin to penetrate into mouse cartilage. Interestingly, statins including simvastatin increase bone mineral density and decrease the risk of fractures in osteoporotic and elderly patients [58–60]. In addition, simvastatin stimulated bone formation in ovariectomized rats [61]. These studies suggest that bone diseases, aging or hormonal disruption, may facilitate the penetration of statins into bone tissue.

We previously demonstrated that statins can effectively inhibit MB cell proliferation and tumor growth by repressing Hh pathway activation. Our studies reveal the synergistic effects of vismodegib and statins in MB cell inhibition, with the strongest synergism found at low doses of vismodegib. Therefore, when used in combination, statins may reduce the dose of vismodegib required for MB treatment, thereby preventing side effects of vismodegib. Here, we further establish that statins caused no defects in bone development, despite the critical role of cholesterol in chondrocyte proliferation and differentiation. Insufficient penetration of statins into the bone contributes to the lack of bone toxicities associated with statins treatment. Our studies provide a strong rationale for the use of statins in the treatment of Hh pathway tumors including MB and BCC. This may be of particular important in the aggressive pediatric Hh-MB subset that currently cannot be treated with Smo inhibitors because of the risk of bone toxicity. Recently four subtypes of SHH-MB have been reported: α, β, γ, and δ [62, 63]. SHH-α subtype mainly affect children (age 3–16). SHH-β and SHH-γ subtypes occur primarily in infants (age <3) [64]. Statins may be warranted for these infant and young patients in that they are vulnerable to bone toxicity associated with Hh pathway inhibition.

Materials and methods

Animal

All mice were maintained under barrier conditions in the Laboratory Animal Facility at Fox Chase Cancer Center, and all experiments were performed in accordance with the procedures approved by the Fox Chase Cancer Center Animal Care and Use Committee. *NSDHL*$^{fl/fl}$ mice were kindly provided by Dr. Gail Herman (The Ohio State University, Columbus, OH); *Sox9-CreER*^{T2} mice were provided by Dr. Maike Sander at the University of California at San Diego. *Math1-Cre* mice, *Rosa-tdTomato* mice, and *Ptch1*$^{fl/fl}$ mice were purchased from The Jackson Laboratory.

Drug treatment

The following compounds were used for our in vitro and in vivo studies: simvastatin (Cayman Chemicals), atorvastatin (Cayman Chemicals), vismodegib (Chemleader Biochemical), WSC (cholesterol-methyl-beta-cyclodextrin; Sigma-Aldrich), and tamoxifen (Sigma-Aldrich, T5648).

Shh conditioned medium (Shh-CM) was prepared by transfection of pcDNA3.1 Shh-N (Addgene) plasmid into 293FT cells. Briefly, 293FT packaging cells were transfected with 2 M $CaCl_2$ and incubated for 8 h before replacing the culture media with 10 ml of Dulbecco's modified Eagle's medium (DMEM) complete medium with 2–5 mM sodium butyrate. The supernatant was harvested at 48 h and 72 h following the transfection and used at 15% for treating chondrocytes.

Simvastatin, atorvastatin, or vismodegib were dissolved in dimethyl sulfoxide (DMSO) as stock solutions (200 mg/ml). Simvastatin DMSO stock was then dissolved in a mixture of ethanol and 0.5% methylcellulose with 0.2% Tween-80 (MCT) and administered at the designated dose by oral gavage. Vismodegib DMSO was also dissolved in MCT. The mixture of DMSO, 0.5% methylcellulose; and 0.2% Tween-80 was used as a vehicle substance.

Tamoxifen was dissolved at a concentration of 20 mg/ml in corn oil and administered intraperitoneally with 0.2 mg daily at postnatal day 10 (P10), once a day for four consecutive days (P10–P14). Animals were sacrificed for further analyses at P16. In our experiments, *Sox9-CreER*^{T2} mice were used as controls for *Sox9-CreER*^{T2}*/NSDHL*$^{fl/fl}$ mice. Control mice and mutant mice were littermates, which were all treated with tamoxifen.

Cell inhibition assay

Simvastatin, atorvastatin, vismodegib, and cisplatin were dissolved in DMSO to a concentration of 10 mM and stored in −20 °C. MB cells were freshly isolated from *Math1-Cre/Ptch1*$^{fl/fl}$ mice at 6 weeks of age, and seeded in a 96-wells plate at a density of 5×10^5 MB cells/well. After drug or DMSO treatment for 48 h, 10 µl of Cell Counting Kit-8 solution (CCK8) was added to each well and further incubated for 2 h. Then, the absorbance values were detected at a wavelength of 450 nm using a Bio-Rad microplate reader. The cell inhibition was calculated by the optical density (OD) values of treated groups/OD values of control groups × 100%.

Synergy determination by the SynergyFinder method

MB cells were seeded in a 96-wells plate at a density of $5{\times}10^5$ MB cells/well, and treated with vismodegib (0, 1, 5, 20, 30, and 50 nM) together with simvastatin or atorvastatin (0, 1, 5, 10, 20, and 30 nM), or cisplatin (0, 1, 3.5, 5, 7, and 10 µM) for 48 h. CCK8 was used to measure the cell inhibition as mentioned above. Synergy scores were determined by the "inhibition readout" using the online SynergyFinder software (https://synergyfinder.fimm.fi) [34] and the ZIP calculation method [35].

Tumor volume measurement

Cerebella of *Math1-Cre/Ptch1*$^{fl/fl}$ mice were scanned by MRI, and DICOM data from MRI sagittal sections were analyzed by DICOM Viewer (GE Healthcare). Briefly, cerebellar area in all sections was measured and the volume of the cerebellum (tumor) was calculated by linear interpolation based on the tissue area and slice thickness.

Primary chondrocytes culture

Chondrocytes were cultured as previously reported [65]. Briefly, wild-type pups at P5 were sacrificed under general anesthesia. Skin and muscles were removed and cartilage tissues washed by PBS for twice. The samples were then incubated with 3 mg/ml collagenase D (Roche) in DMEM (Gibco) at 37 °C for 1.5 h until all soft tissues had detached from the cartilage. The cartilage was then digested with 0.5 mg/ml collagenase D at 37 °C overnight in a Petri dish. Undigested bony parts were discarded and chondrocytes were collected by centrifugation and washed twice with PBS. The primary chondrocytes were cultured in 10% fetal bovine serum (FBS) medium (DMEM, 10% FBS) for 5 days until confluent. Chondrocytes were starved in DMEM with 0.1%FBS for 8 h before treated with Hh-CM or drugs. Chondrocytes were harvested after 48 h treatment for further immunostatining or mRNA evaluation.

Immunofluorescence and immunohistochemistry

For immunofluorescence staining, mice were injected with EdU (100 mg/kg) in PBS 1 h before being sacrificed. Cerebella were fixed overnight in 4% PFA, cryoprotected in 30% sucrose, then frozen in Tissue Tek-OCT (Sakura Finetek, CA) and cut into 12 μm sagittal sections. Bone joint samples were fixed in 4% PFA overnight and decalcified in formic acid and sodium citrate solution for 2 h at room temperature. Bone tissues were embedded in OCT and thin sections (10 μm) were stained with antibodies against Col2 or Sox9. EdU staining was carried out according to the manufacturer's protocol (Carbosynth, NE08701). Sections were counterstained with DAPI and mounted with Fluoromount G (Southern Biotechnology, AL) before being visualized using a Nikon Eclipse Ti microscope. For Immunohistochemistry, bone tissues were decalcified in formic acid and sodium citrate solution for 2 h at room temperature, and then embedded in paraffin. Thin sections (5 μm) were stained with hematoxylin and eosin (H&E) according to the standard protocols. Safranin O staining was performed in the 0.05% fast green (FCF) and 0.1% safranin O solutions (Sigma).

Antibodies used in this study include cleaved caspase-3 (1:200, Cell Signaling, CST9661), collagen 2 (1:500, Abcam, ab34712), Ki67 (1:200, Abcam, ab15580), Sox9 (1:500, abcam, ab185966), collagen X (1:200, Abcam, ab58632).

Q-PCR and genomic PCR

RNA was isolated using TRI reagent (Sigma-Aldrich) in RNase-free conditions. cDNA was synthesized using oligo(dT) and Superscript II reverse transcriptase (Invitrogen). Q-PCR reactions were performed in triplicates using PowerUp™ SYBR™ Green Master Mix (Thermo Fisher) and the Applied Biosystems Real-Time PCR Detection System. In some experiments, genomic DNA was isolated from tissue using DNeasy blood and tissue kit (Qiagen). PCR reactions were performed on a Bio-Rad C1000 touch™ Thermal Cycler. Primer sequences are as follows.

Gene	sequence
SLCO1A2-F	CGCAGGATCCATCAGAGTGT
SLCO1A2-R	CCAAAGGCAGGATGGGAGTT
SLCO2B1-F	TGACTGCTCTCAAAGCCCAG
SLCO2B1-R	CCCTCACCTGTTCTTCCCAA
SLCO1B3-F	GGTGAATGCCCAAGAGACCA
SLCO1B3-R	TGGAGCTAGCATTCCTCCTAGT

PET-CT and MRI

Bone CT images were taken under anesthesia by the Sofie G8 PET-CT system. The mice were positioned within the scanner, and were visually monitored through the scan. During CT scans, the animals were imaged using X-rays. Post-scanning analysis was performed by VivoQuantTM software to measure the length of femur and tibia.

For all MRI studies, anesthesia was carried out using ketamine (100 mg/kg). All mice were kept in a supine position. Tumor-bearing mice were sagittal scanned in a GE MRI scanner. MRI analyses were performed using a T2-FSE (fast spin echo) sequence. Some parameters were TR (repetition time): 3450 ms; TE (echo time): 159 ms; 12 slices of 0.8 mm per slice. Generated images were analyzed employing media viewer (GE Healthcare).

Cholesterol measurement

Cholesterol concentration was measured enzymatically using an Amplex-Red cholesterol assay kit (Thermo Fisher) according to the manufacturer' recommendation. Tissues or cells were dissociated in a lysis buffer containing 1% sodium cholate, 0.1% Triton X-100, 0.1 M potassium phosphate, 0.05 M NaCl, and 100U/ml DNase. The lysate was then shaken at room temperature for 30 min and heated at 60 °C for 30 min, before being applied for cholesterol measurement. The cholesterol concentration was normalized by the amount of total proteins in tissues.

HPLC-MS analyses

Four wild-type mice at P10 were used to detect the presence of vismodegib, simvastatin (SIV), and simvastatin acid by HPLC-MS analyses each time. Mice were sacrificed 30 min following oral treatment of simvastatin (100 mg/kg) or vismodegib (50 mg/kg). The plasma, cerebellar or cartilage homogenates were collected and mixed with 200 μl of acetonitrile in a plastic centrifuge tube and agitated for 2 min in a shaker. Separation of the phase from precipitate was achieved by centrifugation. The supernatant was transferred to a second tube. Fresh acetonitrile (200 μl) was added to the first tube and the same extraction procedure was repeated twice. The supernatants collected from the extractions of the same sample were pooled. This fraction was finally centrifuged, evaporated, and reconstituted with acetonitrile, which was injected into a Waters LC-MS system. The Waters LC-MS system included 2545 binary gradient pump module, 3100 single quadrupole mass detector with electrospray ionization and 2487 UV detector set to 238 nm for SIV and SVA and to 264 nm for vismodegib. HPLC was carried out using a Waters Delta Pak C-18 15u 100A 3.9 ×300 mm column at a flow rate of 0.8 ml/

min, and running a 5% to 95% linear gradient of acetonitrile (0.05% formic acid) over 15 min.

Statistical analysis

All studies were performed at least in five independent replicates with outcomes reflected on photographs or graphs. No specific randomization methods were used in this study. During data analysis, no exclusion criteria were applied. Two-sided Student's *t*-tests were performed to determine the statistical significance of the difference in means between samples in the experiments reported. $P < 0.05$ was considered statistically significant ($*p < 0.05$; $**p < 0.01$; $***p < 0.001$; $****p < 0.0001$; ns, not significant). Unless stated otherwise, data handling and statistical processing were performed using Microsoft Excel.

Acknowledgements We would like to thank Drs. Andrey Efimov, Kathy Cai, Dusica Cvetkovic, and James Oesterling for technical assistance; and Drs. Maike Sander, Joan Font-Burgada, and Sergei Grivenniko for providing transgenic mice. This research was supported by American Cancer Society (RSG1605301NEC to Z.-j.Y.), American Brain Tumor Association (DG1900025 to Z.-j.Y.), PA CURE Health Research Fund (CURE 4100068716 to Z.-j.Y.), National Natural Science Foundation of China (81803616 to C.Z.), and the Natural Science Foundation of Jiangsu Higher Education Institutions (18KJB350010 to C.Z.).

Compliance with ethical standards

Conflict of interest The authors declare no competing interests.

Publisher's note Springer Nature remains neutral with regard to jurisdictional claims in published maps and institutional affiliations.

References

1. Ingham PW, McMahon AP. Hedgehog signaling in animal development: paradigms and principles. Genes Dev. 2001; 15:3059–87.
2. Yang ZJ, Ellis T, Markant SL, Read TA, Kessler JD, Bourboulas M, et al. Medulloblastoma can be initiated by deletion of Patched in lineage-restricted progenitors or stem cells. Cancer Cell. 2008;14:135–45.
3. Ohba S. et al. Hedgehog signaling in endochondral ossification. J Dev Biol. 2016;4:20.
4. Yang J, Andre P, Ye L, Yang YZ. The Hedgehog signalling pathway in bone formation. Int J Oral Sci. 2015;7:73–79.
5. Kan C, Chen L, Hu Y, Ding N, Li Y, McGuire TL, et al. Gli1-labeled adult mesenchymal stem/progenitor cells and hedgehog signaling contribute to endochondral heterotopic ossification. Bone. 2018;109:71–79.
6. Kronenberg HM. Developmental regulation of the growth plate. Nature. 2003;423:332–6.
7. Long F, Zhang XM, Karp S, Yang Y, McMahon AP. Genetic manipulation of hedgehog signaling in the endochondral skeleton reveals a direct role in the regulation of chondrocyte proliferation. Development. 2001;128:5099–108.
8. St-Jacques B, Hammerschmidt M, McMahon AP. Indian hedgehog signaling regulates proliferation and differentiation of chondrocytes and is essential for bone formation. Genes Dev. 1999;13:2072–86.
9. Ng JM, Curran T. The Hedgehog's tale: developing strategies for targeting cancer. Nat Rev Cancer. 2011;11:493–501.
10. Northcott PA, Korshunov A, Witt H, Hielscher T, Eberhart CG, Mack S, et al. Medulloblastoma comprises four distinct molecular variants. J Clin Oncol. 2011;29:1408–14.
11. Thompson MC, Fuller C, Hogg TL, Dalton J, Finkelstein D, Lau CC, et al. Genomics identifies medulloblastoma subgroups that are enriched for specific genetic alterations. J Clin Oncol. 2006;24:1924–31.
12. Gajjar A, Stewart CF, Ellison DW, Kaste S, Kun LE, Packer RJ, et al. Phase I study of vismodegib in children with recurrent or refractory medulloblastoma: a pediatric brain tumor consortium study. Clin Cancer Res. 2013;19:6305–12.
13. Rudin CM, Hann CL, Laterra J, Yauch RL, Callahan CA, Fu L, et al. Treatment of medulloblastoma with hedgehog pathway inhibitor GDC-0449. N Engl J Med. 2009;361:1173–8.
14. Atwood SX, Sarin KY, Whitson RJ, Li JR, Kim G, Rezaee M, et al. Smoothened variants explain the majority of drug resistance in basal cell carcinoma. Cancer Cell. 2015;27:342–53.
15. Sharpe HJ, Pau G, Dijkgraaf GJ, Basset-Seguin N, Modrusan Z, Januario T, et al. Genomic analysis of smoothened inhibitor resistance in basal cell carcinoma. Cancer Cell. 2015;27:327–41.
16. Curran T. Reproducibility of academic preclinical translational research: lessons from the development of Hedgehog pathway inhibitors to treat cancer. Open Biol. 2018;8:180098.
17. Lee Y, Kawagoe R, Sasai K, Li Y, Russell HR, Curran T, et al. Loss of suppressor-of-fused function promotes tumorigenesis. Oncogene. 2007;26:6442–7.
18. Kimura H, Ng JM, Curran T. Transient inhibition of the Hedgehog pathway in young mice causes permanent defects in bone structure. Cancer Cell. 2008;13:249–60.
19. Kieran MW, Chisholm J, Casanova M, Brandes AA, Aerts I, Bouffet E, et al. Phase I study of oral sonidegib (LDE225) in pediatric brain and solid tumors and a phase II study in children and adults with relapsed medulloblastoma. Neuro Oncol. 2017;19:1542–52.
20. Robinson GW, Kaste SC, Chemaitilly W, Bowers DC, Laughton S, Smith A, et al. Irreversible growth plate fusions in children with medulloblastoma treated with a targeted hedgehog pathway inhibitor. Oncotarget. 2017;8:69295–302.
21. Goldstein JL, Brown MS. Regulation of the mevalonate pathway. Nature. 1990;343:425–30.
22. Konig A, Happle R, Bornholdt D, Engel H, Grzeschik KH. Mutations in the NSDHL gene, encoding a 3beta-hydroxysteroid dehydrogenase, cause CHILD syndrome. Am J Med Genet. 2000;90:339–46.
23. Liu XY, Dangel AW, Kelley RI, Zhao W, Denny P, Botcherby M, et al. The gene mutated in bare patches and striated mice encodes a novel 3beta-hydroxysteroid dehydrogenase. Nat Genet. 1999;22:182–7.
24. Lee JJ, Ekker SC, von Kessler DP, Porter JA, Sun BI, Beachy PA. Autoproteolysis in hedgehog protein biogenesis. Science. 1994;266:1528–37.
25. Lewis PM, Dunn MP, McMahon JA, Logan M, Martin JF, St-Jacques B, et al. Cholesterol modification of sonic hedgehog is required for long-range signaling activity and effective modulation of signaling by Ptc1. Cell. 2001;105:599–612.
26. Huang P, Nedelcu D, Watanabe M, Jao C, Kim Y, Liu J, et al. Cellular cholesterol directly activates smoothened in Hedgehog signaling. Cell. 2016;166:1176–87. e1114.
27. Luchetti G, Sircar R, Kong JH, Nachtergaele S, Sagner A, Byrne EF. Cholesterol activates the G-protein coupled receptor Smoothened to promote Hedgehog signaling. Elife. 2016;5:e20304.
28. Byrne EFX, Sircar R, Miller PS, Hedger G, Luchetti G, Nachtergaele S, et al. Structural basis of Smoothened regulation by its extracellular domains. Nature. 2016;535:517–22.

29. Gordon RE, Zhang L, Peri S, Kuo YM, Du F, Egleston BL, et al. Statins synergize with hedgehog pathway inhibitors for treatment of medulloblastoma. Clin Cancer Res. 2018;24:1375–88.
30. Hedger G, Koldso H, Chavent M, Siebold C, Rohatgi R, Sansom MSP. Cholesterol interaction sites on the transmembrane domain of the Hedgehog signal transducer and class F G protein-coupled receptor Smoothened. Structure. 2019;27:549–59. e542.
31. Myers BR, Neahring L, Zhang Y, Roberts KJ, Beachy PA. Rapid, direct activity assays for Smoothened reveal Hedgehog pathway regulation by membrane cholesterol and extracellular sodium. Proc Natl Acad Sci USA. 2017;114:E11141–50.
32. He L, Kulesskiy E, Saarela J, Turunen L, Wennerberg K, Aittokallio T, et al. Methods for high-throughput drug combination screening and synergy scoring. Methods Mol Biol. 2018;1711:351–98.
33. Ianevski A, Giri AK, Aittokallio T. SynergyFinder 2.0: visual analytics of multi-drug combination synergies. Nucleic Acids Res. 2020;48:W488–W493.
34. Ianevski A, He L, Aittokallio T, Tang J. SynergyFinder: a web application for analyzing drug combination dose-response matrix data. Bioinformatics. 2020;36:2645.
35. Yadav B, Wennerberg K, Aittokallio T, Tang J. Searching for drug synergy in complex dose-response landscapes using an interaction potency model. Comput Struct Biotechnol J. 2015;13:504–13.
36. Bosnakovski D, Mizuno M, Kim G, Takagi S, Okumura M, Fujinaga T. Chondrogenic differentiation of bovine bone marrow mesenchymal stem cells (MSCs) in different hydrogels: influence of collagen type II extracellular matrix on MSC chondrogenesis. Biotechnol Bioeng. 2006;93:1152–63.
37. Kalliokoski A, Niemi M. Impact of OATP transporters on pharmacokinetics. Br J Pharmacol. 2009;158:693–705.
38. Kellick KA, Bottorff M, Toth PP. The National Lipid Association's Safety Task Force. A clinician's guide to statin drug-drug interactions. J Clin Lipidol. 2014;8:S30–46.
39. Roth M, Obaidat A, Hagenbuch B. OATPs, OATs and OCTs: the organic anion and cation transporters of the SLCO and SLC22A gene superfamilies. Br J Pharmacol. 2012;165:1260–87.
40. Kopp JL, Dubois CL, Schaffer AE, Hao E, Shih HP, Seymour PA, et al. Sox9+ ductal cells are multipotent progenitors throughout development but do not produce new endocrine cells in the normal or injured adult pancreas. Development. 2011;138:653–65.
41. Madisen L, Zwingman TA, Sunkin SM, Oh SW, Zariwala HA, Gu H, et al. A robust and high-throughput Cre reporting and characterization system for the whole mouse brain. Nat Neurosci. 2010;13:133–40.
42. Cunningham D, DeBarber AE, Bir N, Binkley L, Merkens LS, Steiner RD, et al. Analysis of hedgehog signaling in cerebellar granule cell precursors in a conditional Nsdhl allele demonstrates an essential role for cholesterol in postnatal CNS development. Hum Mol Genet. 2015;24:2808–25.
43. Tsushima H, Tang YJ, Puviindran V, Hsu SC, Nadesan P, Yu C, et al. Intracellular biosynthesis of lipids and cholesterol by Scap and Insig in mesenchymal cells regulates long bone growth and chondrocyte homeostasis. Development. 2018;145:dev162396.
44. Duggan DE, Vickers S. Physiological disposition of HMG-CoA-reductase inhibitors. Drug Metab Rev. 1990;22:333–62.
45. Kantola T, Kivisto KT, Neuvonen PJ. Grapefruit juice greatly increases serum concentrations of lovastatin and lovastatin acid. Clin Pharm Ther. 1998;63:397–402.
46. Lilja JJ, Kivisto KT, Neuvonen PJ. Grapefruit juice-simvastatin interaction: effect on serum concentrations of simvastatin, simvastatin acid, and HMG-CoA reductase inhibitors. Clin Pharm Ther. 1998;64:477–83.
47. Schachter M. Chemical, pharmacokinetic and pharmacodynamic properties of statins: an update. Fundam Clin Pharmacol. 2005;19:117–25.
48. Rocha VZ, Santos RD. Safety of statin treatment in children with familial hypercholesterolemia: filling the gaps. J Clin Lipidol. 2018;12:12–15.
49. Kusters DM, Avis HJ, de Groot E, Wijburg FA, Kastelein JJ, Wiegman A, et al. Ten-year follow-up after initiation of statin therapy in children with familial hypercholesterolemia. JAMA. 2014;312:1055–7.
50. Haraguchi R, Kitazawa R, Kohara Y, Ikedo A, Imai Y, Kitazawa S. Recent insights into long bone development: central role of Hedgehog signaling pathway in regulating growth plate. Int J Mol Sci. 2019;20.
51. Suzuki A, Ogata K, Yoshioka H, Shim J, Wassif CA, Porter FD, et al. Disruption of Dhcr7 and Insig1/2 in cholesterol metabolism causes defects in bone formation and homeostasis through primary cilium formation. Bone Res. 2020;8:1.
52. Maeda Y, Nakamura E, Nguyen MT, Suva LJ, Swain FL, Razzaque MS, et al. Indian Hedgehog produced by postnatal chondrocytes is essential for maintaining a growth plate and trabecular bone. Proc Natl Acad Sci USA. 2007;104:6382–7.
53. Xu R, Khan SK, Zhou T, Gao B, Zhou Y, Zhou X, et al. Galphas signaling controls intramembranous ossification during cranial bone development by regulating both Hedgehog and Wnt/beta-catenin signaling. Bone Res. 2018;6:33.
54. Gofflot F, Hars C, Illien F, Chevy F, Wolf C, Picard JJ, et al. Molecular mechanisms underlying limb anomalies associated with cholesterol deficiency during gestation: implications of Hedgehog signaling. Hum Mol Genet. 2003;12:1187–98.
55. Wu S, De Luca F. Role of cholesterol in the regulation of growth plate chondrogenesis and longitudinal bone growth. J Biol Chem. 2004;279:4642–7.
56. Laughlin RC, Carey TF. Cataracts in patients treated with triparanol. JAMA. 1962;181:339–40.
57. Roux C, Dupuis R, Horvath C, Talbot JN. Teratogenic effect of an inhibitor of cholesterol synthesis (AY 9944) in rats: correlation with maternal cholesterolemia. J Nutr. 1980;110:2310–2.
58. Chan KA, Andrade SE, Boles M, Buist DS, Chase GA, Donahue JG, et al. Inhibitors of hydroxymethylglutaryl-coenzyme A reductase and risk of fracture among older women. Lancet. 2000;355:2185–8.
59. Maeda T, Kawane T, Horiuchi N. Statins augment vascular endothelial growth factor expression in osteoblastic cells via inhibition of protein prenylation. Endocrinology. 2003;144:681–92.
60. Wang PS, Solomon DH, Mogun H, Avorn J. HMG-CoA reductase inhibitors and the risk of hip fractures in elderly patients. JAMA. 2000;283:3211–6.
61. Mundy G, Garrett R, Harris S, Chan J, Chen D, Rossini G, et al. Stimulation of bone formation in vitro and in rodents by statins. Science. 1999;286:1946–9.
62. Cavalli FMG, Remke M, Rampasek L, Peacock J, Shih DJH, Luu B, et al. Intertumoral heterogeneity within medulloblastoma subgroups. Cancer Cell. 2017;31:737–54. e736.
63. Schwalbe EC, Lindsey JC, Nakjang S, Crosier S, Smith AJ, Hicks D, et al. Novel molecular subgroups for clinical classification and outcome prediction in childhood medulloblastoma: a cohort study. Lancet Oncol. 2017;18:958–71.
64. Hovestadt V, Ayrault O, Swartling FJ, Robinson GW, Pfister SM, Northcott PA. Medulloblastomics revisited: biological and clinical insights from thousands of patients. Nat Rev Cancer. 2020;20:42–56.
65. Gosset M, Berenbaum F, Thirion S, Jacques C. Primary culture and phenotyping of murine chondrocytes. Nat Protoc. 2008; 3:1253–60.